J. Non-crystalline Solids, 358(4):721–727, 2012.

Sol-Gel Simulation–I: Scattering Response

F. A. Campo[1] and
E. J. Barbero[2] and Mechanical and Aerospace Engineering, West Virginia University, Morgantown, WV 26506-6106, USA

1 Abstract

Scattering of sol-gel structures is investigated computationally. Sol-gels are recreated through an aggregation algorithm incorporating Brownian motion and chemical reactions. Using the fractal character of sol-gels, the concept of recursion is introduced as a tool to perform multi scale computation of the response of sol-gels through the different scales from the molecular level to the macro scale. The concept is illustrated with the prediction of scattering intensity. The relationship between scattering intensity and functionality is investigated, noting that the later is a function of the Brownian motion and chemical reactivity. Computational simulation tools are developed to predict scattering intensity as a function of density and reactivity, the former represented by the number of particles, or clusters, in the simulation box. Then, the results are correlated to an analytical model that reveals the critical wave number, or critical scale, at which percolation occurs.

Keywords

Aggregation; Aerogel; Multi Scale; Percolation; Fractal

2 Introduction

Advanced products such as dense films, Aerogels, super capacitors, and dense ceramics can be fabricated with Sol-gel technology [1,4,8,12,22,28,31,32,34]. This technology uses colloidal aggregation [3,5–7,9,11,13,14,24–26,30,33,35,36,38,39,42], which after the removal of the liquid phase leaves a solid ceramic structure [21,38]. Extracting the liquid phase of the colloid gently, e.g. by supercritical drying, leaves a solid structure with unique physical properties [12,21,30,41,42].

The outstanding properties of gel-derived materials are the result of a) the physical properties of the base material and b) the unique structure of the resulting material [9,15]. To characterize the structure of gel-derived materials, Small Angle Neutron Scattering (SANS) and Small Angle X-Ray Scattering (SAXS) have been used extensively [10,16–20,38,40,41] revealing their fractal structure along several length scales [38].

In many cases, physical properties of the gel-derived structures can be explained by their fractal structure [9,15]. However, fractal theory is not always applicable, in particular when it becomes

[1]Graduate Research Assistant

[2]Corresponding author. The final publication is available at http://dx.doi.org/10.1016/j.jnoncrysol.2011.10.023

(a) $(w, N) = (0.1, 100)$ (b) $(w, N) = (1.6, 100)$

Figure 1: Cross-section of an aggregated structure inside the simulation box, at scale $\lambda \in [1, \lambda_{max}]$.

inadequate to associate a fractal range to the structure, or when within a proved fractal range the response is not explained by classical fractal theory [40, 41].

In this work, it is proposed that some responses of gel-derived materials depend on the connectivity of the structure while other responses depend on the mass distribution of the structure. In this manuscript, density and scattering intensity are shown to depend on the mass distribution. For this, density and scattering intensity of computer generated structures that resemble gels and Aerogels are evaluated. On the other hand, Mechanical response of gels and Aerogels and their relationship to scattering are investigated in Part II [2].

3 Computer-generated Structures

The structures at scale $\lambda \in [1, \lambda_{max}]$ are generated by an aggregation algorithm explained in detail in [6]. Here λ_{max} stands for the maximum scale at the first generation of the multi scale algorithm, a scale that is given by the size of the simulation box $L = \lambda_{max}(2a_0)$, where $2a_0$ is the size of the primary particles. First, particles are randomly positioned at the sites of a cubic lattice inside the simulation box. Then, a particle is chosen randomly to move in the lattice, in order to reproduce the Brownian motion that occurs in a forming colloid satisfying Einstein-Smoluchowsky theory [29, 37]. For two colliding particles, the probability of forming a bond is determined by the reactivity ω and their coordination numbers n_{cA} and n_{cB}. If the bond is formed, the clusters containing the colliding particles bond into a single, larger cluster. Periodic Boundary Conditions (PBC) are used to delimit the simulation box. The algorithm ends when all particles form a single cluster. At this point we say that all particles have aggregated, which is not the same as saying that all particles have bonded with their neighbors. For that one would have to age/sinter the structure. Typical structures are depicted in Figure 1 for low and high reactivity w.

Reactivity is a measure of the increase or decrease of additional energy required to form a new bond as a function of the number of bonds already formed. Using this concept, the probability of reaction of two particles is calculated using the the Metropolis algorithm [6]. In this way, different structures are formed by varying the reactivity. Longer branched structures are formed for lower reactivities, and more compact structures are formed for higher reactivities. The particular case of neutral Aerogels was found to correspond to a reactivity of $w = 1$.

The resulting structure has a functionality[3] distribution which not always coincides with the coordination number[4] distribution. However, both distributions can be modified as follows. When

[3]The functionality counts how many particles are next to a particle.

[4]The coordination number counts how many particles are bonded to a particle.

sintering and/or aging a sol, the coordination number distribution approaches the functionality distribution, as bonds appear between the particles that are next to each other. Also, as the initial density is lowered, the functionality distribution approaches the coordination number distribution (since all particles that are neighbors tend to bond when the density is low). Thus, responses such as stiffness, which are associated to the connectivity of the structure, are expected to be related to the coordination number rather than to the mass distribution, which is measured by the functionality. On the other hand, responses such as scattering intensity, which are associated to mass distribution, are expected to be related to functionality.

In this paper, scattering intensity (as a measure of mass distribution) is investigated for sol-gels. Mechanical properties (as a measure of the connectivity of the structure) and their relationship to scattering, are investigated in Part II [2].

4 Correlation Length

The correlation length ξ is a measure of the size of the clusters that have aggregated during the gelation process. The relation between correlation length and density of the cluster is developed in this section for structures with constant fractal dimension. In a simulation box of size L, the aggregation process initially consists of N_0 primary particles of size $2a_0$ that aggregate. The primary particles may be molecules like SiO_2, or cluster of molecules with a known size and density. The effective density is $\rho_{ef}^0 = N_0/L^3$, where N_0 is the number of particles in the simulation box. Conservation of mass implies that the effective density is constant through the aggregation process. However, during aggregation, gaps are created as the clusters bond without perfect match. Therefore, the density of the forming clusters decreases due to the incorporation of vacancies, the size of the clusters ξ increases, and the number of clusters N_C decreases. Due to the decrease in the number of clusters in the simulation box, the average distance between clusters d increases. In this way, the density of the cluster can be calculated as

$$\rho_C = \frac{N_C}{L^3} = \frac{1}{d^3} \tag{1}$$

Note that the number of particles N_0 can be calculated as

$$N_0 = N_C \; N_{k/C} \tag{2}$$

where $N_{k/C}$ is the number of particles per cluster. Furthermore, assuming that the aggregation process leads to a fractal structure, $N_{k/C}$ follows a power law as

$$N_{k/C} = \left(\frac{\xi}{2a_0}\right)^{\mathcal{D}} \tag{3}$$

where $\mathcal{D}$ is the fractal dimension of the of the clusters.

At the end of the aggregation process, when only one cluster is found inside the simulation box, $N_C = 1$. Therefore, (3) can be rewritten as

$$\frac{\xi}{2a_0} = N_0^{1/\mathcal{D}} \tag{4}$$

From (1), it is concluded that the mean free path d becomes equal to the size of the simulation box, i.e. $d = L$.

Note that if $\xi < L$, the structure will not percolate and the effective density N_0/L^3 would be lower than the density of the cluster N_0/ξ^3.

Since ξ is limited by d, the system percolates for $L = \xi = d$, thus defining the critical percolation density

$$\rho_{crit} = \frac{L^{\mathcal{D}-3}}{(2a_0)^{\mathcal{D}}} \tag{5}$$

In other words, if ξ is chosen to be at least d, the cluster spans the entire simulation box, connecting opposite faces of the simulation box. Using a dimensionless system, we have $2a_0 = 1$, $L' = L/(2a_0)$, and $\rho' = (2a_0)^3\rho$ Then, $\rho'_{crit} = L'^{\mathcal{D}-3}$.

5 Percolation Kinematics

In this section, the evolution of a cluster during the aggregation process is described in terms of the number of particles per cluster $N_{k/C}$ and the number of clusters N_C in the simulation box.

The aggregation process is assumed to be isotropic. At time t, in average, there are $N_{k/C}^{(t)}$ particles per cluster and $N_C^{(t)}$ clusters in a simulation box of volume L^3. Let Δt be the time it takes for the clusters to collide and bond with a second cluster, thus doubling the number of particles in each cluster while cutting in half the number of clusters in the simulation box. Then,

$$N_{k/C}^{t+\Delta t} = 2N_{k/C}^{t} \tag{6}$$

$$N_C^{t+\Delta t} = \frac{N_C^t}{2} \tag{7}$$

Using (3) in (6) and (1) in (7), the evolution of the correlation length ξ and the separation between clusters d is given by

$$\xi^{t+\Delta t} = 2^{1/\mathcal{D}}\xi^t \tag{8}$$

$$d^{t+\Delta t} = 2^{1/3}d^t \tag{9}$$

Noting that $d^0 = LN_0^{1/3}$ and $\xi^0 = 2a_0$, the recurrence can be solved for a time $t = n\Delta t$ as

$$\xi^{n\Delta t} = 2^{n/\mathcal{D}_{NC}}(2a_0) \tag{10}$$

$$d^{n\Delta t} = 2^{n/3}LN_0^{-1/3} \tag{11}$$

Since ξ and d share the value n, the parameters are correlated by

$$\xi(t) = 2a_0\left(\frac{d(t)}{LN_0^{-1/3}}\right)^{\frac{3}{\mathcal{D}}} \tag{12}$$

If $\xi(t) = L$ at any time during the aggregation process, the structure percolates. This is the proposed *percolation criterion.*

It can be shown that if the separation between the clusters $d(t)$ is equal to L, when there is only one cluster in the simulation box, the size of the clusters satisfy $\xi(t) = L$, and the structure critically percolates.

When percolation starts at $t = t_{per}$, $\xi(t_{per}) = L$, and the distance between clusters is

$$d(t_{per}) = \left(\frac{N_0}{L^3}\right)^{-1/3} \left(\frac{L}{2a_0}\right)^{\frac{\mathcal{D}}{3}} \tag{13}$$

Note that $d(t = t_{per})$ may be smaller, equal, or greater than L. Thus, the number of clusters $N_C(t = t_{per})$ inside the simulation box can be calculated as

$$N_C(t = t_{per}) = N_0 \left(\frac{2a_0}{L}\right)^{\mathcal{D}} \tag{14}$$

If the percolation criterion is not satisfied ($\xi(t) < L$) with one cluster ($N_C = 1$) aggregating all the particles, then $\xi/(2a_0) = N_0^{(1/D)}$, and $d = L$. The isolated cluster does not percolates.

If the percolation criterion is satisfied ($\xi = L$) with one cluster ($N_C = 1$), the aggregation process ends as soon as the structure percolates ($t = t_{per}$). The cluster aggregates with the fractal dimension of the physical aggregate, unconstrained by the simulation box.

If the percolation criterion is satisfied and $N_C > 1$, then there are multiple clusters still available that can further aggregate. If allowed to further aggregate in a larger simulation box, the final cluster would be larger than the simulation box ($\xi > L$). When constrained by the simulation box, the cluster aggregates with a fractal dimension higher than that of the physical aggregate.

From this discussion, three regimes are identified:

1. When $\xi < L$, isolated clusters are suspended in the simulation box.
2. When $\xi = L$, the density is the critical percolation density, and the structure spans the simulation box.
3. When $\xi > L$, the the structure spans the simulation box before all particles are aggregated.

6 Scattering Intensity

Scattering has been widely used to characterize the structure of aerogels and disordered systems [10, 16–20, 38, 40, 41]. Researchers use scattering techniques to identify the size of the primary particle $2a_0$ and the size of the clusters formed, the later known as the correlation length ξ. Also, scattering experiments support the fractal nature of aerogels by evidencing a power law between the scattered intensity $I(q)$ and the the modulus of the scattering wave vector q

$$I(q) \propto q^{-D_q} \tag{15}$$

where D_q is the fractal dimension associated to the intensity.

The scattering intensity is obtained by multiplying the scattering function[5] $S(q)$ by the form factor[6] $P(q)$ of the scattering centers and the number of particles as follows [10]

$$I(q) = NP(q)S(q) \tag{16}$$

where N is the number of particles. The scattering function $S(q)$ can be calculated as [10]

$$S(q) = \frac{1}{N} \sum_i^N \sum_j^N m_i m_j \frac{\sin(qr_{ij})}{qr_{ij}} \tag{17}$$

[5]The scattering function accounts the interference of the scattered beams caused by the mass distribution of the scattering centers.

[6]The form factor accounts for the scattering of the beam by each of the scattering centers.

where $r_{ij} = |r_i - r_j|$ is the relative distance between the centers, r_i and r_j, for the particles tagged as i and j, and m_i, m_j are the scattering amplitudes proportional to the mass of the scattering centers i and j, respectively.

In (17), $\frac{1}{N}\sum_i$ corresponds to the average over N particles of the total intensity of the interference between the scattered beams by particle i and all the other particles (summation over j).

The calculation of the scattering intensity of large structures can be done using their fractal character. By fractal character it is understood that the structure (mass distribution) is similar at different scales [23, 27]. Similarity implies that for each entity at a certain scale, there is another entity identified in a similar way at a larger scale. Considering a structure at two scales, a small scale $\lambda \in [1, \lambda_{max}]$ and at large scale $\lambda' \in \left[\lambda_{max}, \lambda_{max}^2\right]$, we have

$$\lambda' = \lambda\lambda_{max} \tag{18}$$

where $\lambda_{max} = L_{max}/L_{min}$, L_{min} is the size of the primary particle at the smallest scale of the aggregation process.

The smallest discernible particle is called primary particle. Its properties are those of the precursor material, which in this study is SiO_2. The primary particle is identified at the small scale range at $\lambda = 1$. At any subsequent scale, the primary particle is the cluster generated at the previous scale. This means that the primary particle size at the larger scale is of the size of the cluster at the previous smaller scale. The primary particle at the subsequent scale is named *primary cluster* and is defined at $\lambda' = \lambda_{max}$.

The scattering function (17) is valid for the range

$$\frac{\pi}{2L_{max}} < q < \frac{\pi}{2L_{mim}} \tag{19}$$

where $L_{max} = \lambda_{max}L_{min}$ is the size of the simulation box, and L_{min} is the primary cluster size at each scale. Thus, (19) suggests that the calculation of the scattering intensity can be separated into wave number ranges $\delta_i = [\frac{\pi}{2L_{min}^{(i)}}, \frac{\pi}{2L_{max}^{(i)}}]$.

$$\begin{aligned} L_{min}^{(1)} &= a_0 \\ L_{max}^{(i)} &= \lambda_{max}L_{min}^{(i)} \\ L_{min}^{(i)} &= L_{max}^{(i-1)} \end{aligned} \tag{20}$$

where $2a_0$ is the size of the primary particle.

Equation (20) means that only the structure at the range of scales $\lambda^{(i)} = [\frac{L_{min}^{(i)}}{2a_0}, \frac{L_{max}^{(i)}}{2a_0}]$ is required to calculate (17) instead of requiring all the detail for all scales. This results in significant computational savings. Hence, (16) can be rewritten as

$$I(q) = NS(q)P^{(i)}(q) \tag{21}$$

where $i = \{i : q \in \delta_i\}$. The form factor $P^{(i)}(q)$ corresponds to the form factor of the primary cluster at the scale range (i). Then, it can be reconstructed by *recursion* starting from $P^{(0)} = P_0(q)$ corresponding to the form factor of the primary particles, using

$$P^{(i)}(q) = P^{(i-1)}(q)\left(\frac{\pi/(2L_{max}^{(i)})}{\pi/(2L_{min}^{(i)})}\right)^{-D_q^{(n-1)}} = P^{(i-1)}(q)\lambda_{max}^{D_q^{(n-1)}} \tag{22}$$

with $D_q^{(n-1)}$ the fractal dimension calculated for δ_i

	w						
N	0.1	0.2	0.4	0.8	1.0	1.2	1.6
100	No	No	No	No	No	No	No
200	No	No	No	No	No	No	No
400	Yes	Yes	Yes	No	Yes	No	No
800	Yes	Yes	Yes	Yes	Yes	Yes	Yes
1600	Yes	Yes	Yes	Yes	Yes	Yes	Yes
1728	Yes	Yes	Yes	Yes	Yes	Yes	Yes

Table 1: Percolation results and test conditions. N is the number of particles in the simulation box, and w is the reactivity.

This study assumes $P_0^{(i)}(q) = 1$. Only the scattering function $S(q)$ is required to calculate the scattering intensity for any value of q using (21) and (22).

Scattering intensities for the samples in Table 1 using (17) are shown in Figure 2. In the Figure, D is the fractal dimension calculated from (24) after conditioning the signal with (25), $2a_0$ is the cluster radius, and q is the dimensionless wave number. The scattering profile $I(q)$ predicted by the computational experiment (simulation) is shown with thick solid lines. An approximation using the model described in Section 7 is displayed with thin lines. Among the thin lines, continuous lines indicate percolated structures and discontinuous lines represent non-percolated structures.

7 Analytical Model

An analytical model for the scattering intensity is proposed in this section. The model consists on dividing the scattering range into two intervals: 1) $q < q_{crit}$ where the scattering of the structure resembles the scattering of a continuum solid, and 2) $q > q_{crit}$ where the scattering of the structure resembles the scattering of isolated particles. Based on the three regimens identified in Section 5, the critical percolation wave number q_{crit} is here defined as

$$q_{crit} = \frac{\pi}{2\xi} \tag{23}$$

7.1 Continuum Regime

For a simulation box of volume L^3, if the correlation length is larger than the size of the simulation box, $\xi > L$, the aggregating clusters percolate, thus, for $q < q_{crit}$ the structure looks homogeneous with the fractal dimension of a solid. Since the effective density does not change as a function of the wave number, the measured fractal dimension is $D_q = 3$. Hence, the scattering intensity follows (15), i.e., $I(q) \propto q^{-3}$.

This case is dominant when the number of particles N is large and thus most of the sites are occupied, as illustrated by thin, continuum lines in Figure 2.

7.2 Isolated Clusters Regime

For $q > q_{crit}$, the scattering intensity resembles that of isolated spheres [10, 16] of radius $R = \xi/2$. An attenuation factor $(q/q_0)^{-(3-D_q)}$ is proposed here to take into account the mass reduction due to the fractal character of the clusters. Hence, the proposed scattering intensity model satisfies

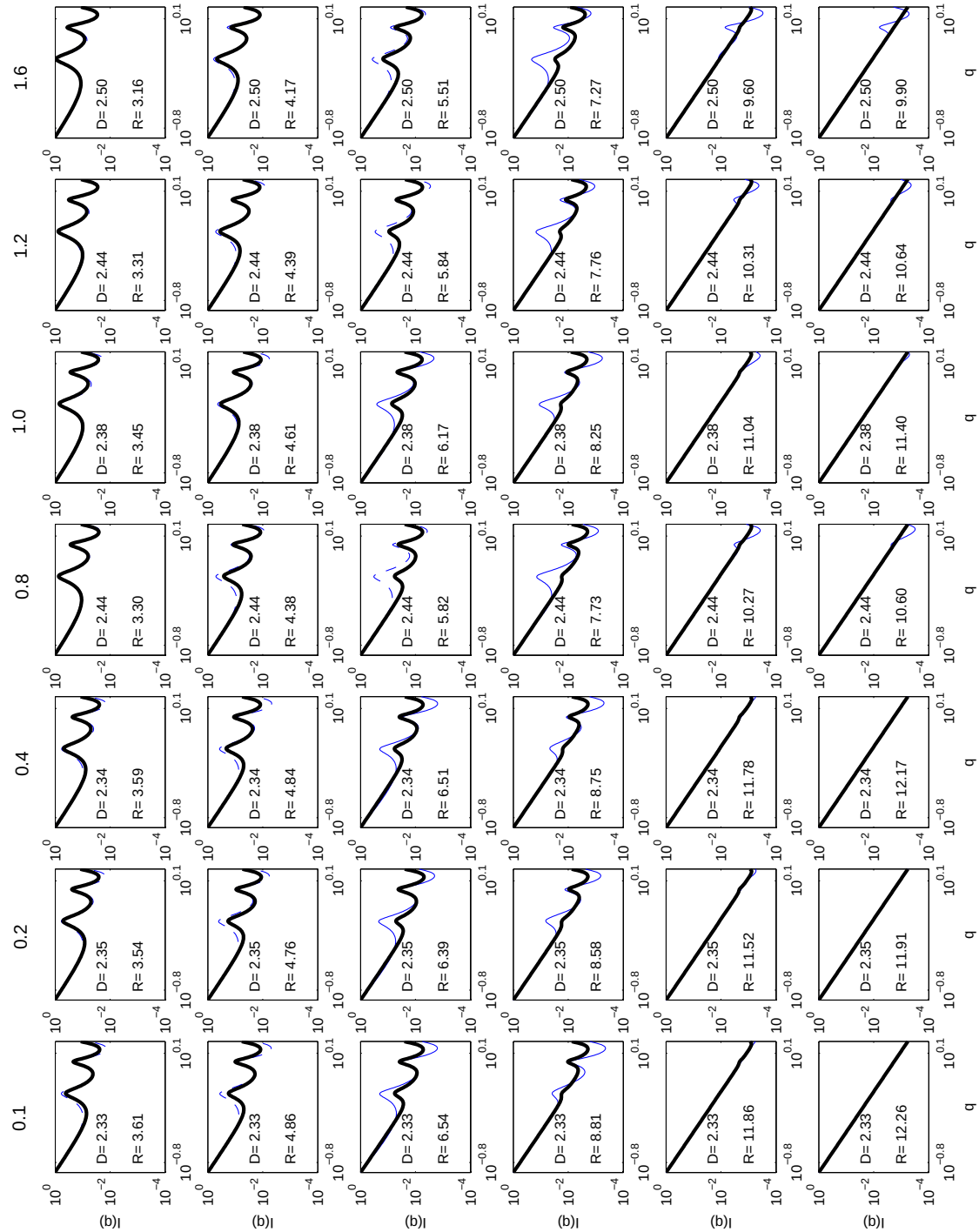

Figure 2: Scattering Intensities for the samples in Table 1. Rows, from top to bottom, correspond to N=100, 200, 400, 800, 1600, and 1728 particles. Columns, from left to right, correspond to reactivities w=0.1, 0.2, 0.4, 0.8, 1.0, 1.2, and 1.6

$$I(q) = \left(3\frac{\sin qR - qR\cos qr}{(qR)^3}\right)^2 \left(\frac{q}{q_0}\right)^{-(D_q-3)} \tag{24}$$

In Figure 2, this regime is illustrated by thin, discontinuous lines. This regime is dominant for low number of particles. In this way, the fractal dimension of the clusters can be determined by fitting (24) to the scattering intensity calculated by the computer simulation (thick, solid lines in the Figure).

Polydispersity, due to the cluster radius variability is incorporated by averaging the scattering intensity (24) for a log-normal distribution of radii, using a procedure similar to [16, 20]. This is made possible by simulating 32 specimens for each of the 42 samples depicted in Figure 2.

7.3 Critical Percolation Regime

The *isolated cluster regime* transitions into the *continuum regime* at the critical percolation state with q_{crit} in the range given by (19). At this state, the structure is a collection of clusters forming a highly porous structure.

In Figure 2, the critical percolation is identintified when q_{crit} enters into the simulation wave number range given by (19), i.e. $2R = L$. Also, during this regime, $D = D_q$.

7.4 Scattering Results

Simulation of scattering intensity is reported in this section. The influence of the reactivity and precursor density on the scattering intensity was investigated by modelling the scattering function of structures recreated using the algorithm described in Section 3. The fractal dimension inside the cluster and the radius of the cluster where measured by fitting the parameters of the analytical model presented in Section 7.

Border effects are removed in the same way they are removed experimentally [10,16]. That is, the measured logarithmic intensity is subtracted from the signal $S_{cube}(q)$ produced by an homogeneous sample, which in this work is a simulation box with all sites occupied (fractal dimension equal to 3). In this way, the reported intensity corresponds to

$$I(q) = I_0 \frac{S(q)}{S_{cube}(q)} \left(\frac{q}{q_0}\right)^{-3} \tag{25}$$

where $I_0 = 1$ for $q_0 = q_{min}$.

The scattering intensity $I(q)$, fractal dimension D_q, and equivalent radius of the clusters R_{eq} are calculated for the conditions in Table 1 and presented in Figure 2. The reported wave number q is dimensionless calculated as $q = 2\pi/\lambda$. Note that since $P(q) = 1$, the scattering intensity and the scattering function have the same values.

Thirty-two samples are used to average[7] the scattering results for each of the 42 conditions studied. Since the most accurate measurement of the fractal dimension occurs for low number of particles, it is assumed that the fractal dimension for larger number of particles is the same, if the reactivity is the same. A standard deviation of 50% of the average cluster radius was used for polydispersity. In order to avoid a discontinuity between the sphere model and the continuous model, a log-linear interpolation is used from the $q_{crit}/2$ to q_{crit}.

Note that the proposed analytical model for scattering intensity fits the behavior well in Figure 2. That is, the thin lines representing the analytical model of Section 7 overlap large regions if not

[7] An average is calculated for the structures generated as the result of aleatory character of the algorithm yielding a polydisperse population of clusters.

all of the simulation results (thick lines). The regions that are not overlapped, are explained by the transition interval of the analytical model from the isolated cluster regime to the continuum regime. Note that there is an increase of the calculated fractal dimension and a reduction of the sphere radius with the increase of reactivity.

The criterion for percolation presented in Section 5 it used to determine if the structures percolated or not, which is then reported in Table 1. A tendency to percolate is observed as the reactivity decreases and the number of particles increases.

8 Discussion

For larger values of q, the small structural features influence the scattering results, whereas for smaller values of q, the larger features are responsible for the scattering intensity. Then, selecting a particular interval of wave numbers allows us to characterize the type of features present at a certain scale interval. However, the scale intervals and the wave number intervals are inversely proportional.

The peaks in Figure 2 are the result of the scattering of the clusters as isolated spheres (or scattering of the pores between the clusters). As the number of particles in the simulation box increases, a continuum phase appears, thus reducing the effect of the pores. As revealed by the analytical model, as the number of particles N increases, the continuum regime becomes dominant compared to the isolated clusters regime. On the other hand, as the number of particles is reduced below the critical percolation density, the isolated clusters regime becomes dominant.

An increase in the number of particles increases the size of the associated cluster since each cluster is made of more particles. However, the fractal dimension of the clusters is not expected to change considerably since the same chemical reactions and Brownian motion occur as long as the clusters do not percolate. That is, for values of $q > q_{crit}$, all structures with the same reactivity have the same fractal dimension regardless of the number of particles.

Structures that become continuum at a certain scale, remain continuum for larger scales. Similarly, structures that do not percolate will remain disconnected at larger scales as well. Only structures that critically percolate can change their regime at larger scales, thus remaining critically percolating, or not percolating, or becoming continuum. Thus, using the recursion in (21) and (22), the scattering intensity can be found for any structure, percolated or not.

As the reactivity increases, more compact structures are observed, congruent with the definition of reactivity and results in [6]. The fractal dimension and critical density[8] $n_0 = N_0/L^3$ as a function of the reactivity for critical percolation are presented in Figure 3. Since higher fractal dimensions correspond to more compact structures, reduced radii are expected for the clusters yielding higher critical densities. For the range of reactivities studied, there is a monotonic increase of fractal dimension and critical density. However, achieving compact structures with fractal dimension of 3 should require infinite reactivity. Furthermore, for reactivities several orders of magnitude smaller, almost linear structures are expected with fractal dimensions close but greater than one.

9 Conclusions

The mass distribution in the sol-gel determines alone the scattering intensity. Then, the fractal character of the mass distribution causes the scattering intensity to have a fractal character as well. Also, the recursion algorithms proposed in order to calculate the effective scattering response of

[8]The critical density is defined as the number of primary particles in the simulation box at the scale range considered.

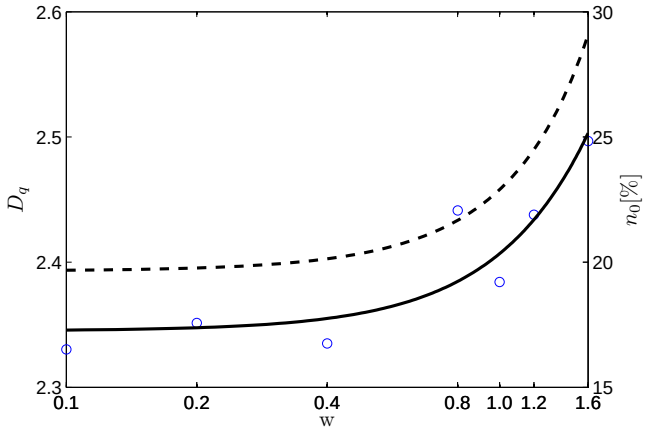

Figure 3: Fractal dimension (continuous line) and critical percolation density (discontinuous line) as a function of reactivity.

the structure at different scale ranges can be used as a consequence of as the mass distribution having fractal character. Therefore, the scattering intensity evaluated at a certain wave number can be understood as the effective form factor of the structure at the corresponding scale. In addition, the effective from factor can be investigated by analyzing the structure in a limited scale range, with a reduced number of particles as compared to solving an involved model spanning a broad range of scales, which would be prohibitively expensive. The results in the behavior of the functionality distribution reported by [6] were confirmed through scattering experiments by comparing the fractal dimensions, and finding higher fractal dimensions, i.e. more compact structures, for higher reactivities.

References

[1] Yu K. Akimov. Fields of application of aerogels (review). *Instrum. Exper. Techniques*, 46:287, 2003.

[2] E. J. Barbero and F. A. Campo. Sol gel simulation–II: Mechanical response. *Computational Materials Science (submitted)*, 2011.

[3] R. Botet, R. Jullien, and M. Kolb. Hierarchical model for irreversible kinetic cluster formation. *J. Phys. A: Math Gen.*, 17:L75–L79, 1984.

[4] C.J. Brinker and G.W. Scherer. *Sol-Gel Science. The Physics and chemistry of Sol-Gel Processing*. Academic Press, New York, USA, 1990.

[5] M.M. Bruno, N.G. Cotella, M.C. Miras, T. Koch, S. Seidler, and C. Barbero. Characterization of monolithic porous carbon prepared from resorcinol/formaldehyde gels with cationic surfactant. *Colloids and Surfaces A: Physicochemical and Engineering Aspects*, 358(1-3):13 – 20, 2010.

[6] F. A. Campo, J. S. Rivas Murillo, and E. J.Barbero. Aggregation model for the gelation of a sol starting from the processing conditions. *J. Non-Cryst. Solids.*, July-2010.

[7] S. Corezzi, D. Fioretto, C. De Michele, E. Zaccarelli, and F. Sciortino. Modeling the crossover between chemically and diffusion-controlled irreversible aggregation in a small-functionality gel-forming system. *The Journal of Physical Chemistry B*, 114(11):3769–3775, March 2010.

[8] G. Dominguez, A.J. Westphal, M. L. F. Phillips, and S.M. Jones. A fluorescent aerogel for capture and identification of interplanetary and interstellar dust. *Astrophys. J*, 592:631–635, 2003.

[9] A. Emmerling and J. Fricke. Scaling properties and structure of aerogels. *Journal of Sol-Gel Science and Technology*, 8:781–788, 1997.

[10] L.A. Feigin and P.I. Svergun. *Structure Analysis by Small Angle X-rays and Neutron scattering.* Plenumm, USA, 1987.

[11] F. Ferri, B.J. Frisken, and D.S. Cannell. Structure of silica gels. *Phys. Rev. Lett.*, 67(25):3626–3629, 1991.

[12] J. Fricke and A. Emmerling. Aerogels - recent progress in production techniques and novel applications. *J. Sol-Gel Sci. Technol.*, 13:299–303, 1998.

[13] D. Fry, A. Mohammad, A. Chakrabarti, and C. M. Sorensen. Cluster shape anisotropy in irreversibly aggregating particulate systems. *Langmuir*, 20(18):7871–7879, August 2004.

[14] Agustin E. Gonzalez and Guillermo Ramirez-Santiago. Scaling of the structure factor in fractal aggregation of colloids: Computer simulations. *Journal of Colloid and Interface Science*, 182:254–267, 1996.

[15] J. Gross and J. Fricke. Scaling of elastic properties in highly porous nanostructured aerogels. *NanoStructured Materials*, 6:905–908, 1995.

[16] Boualem Hammouda. *Probing Nanoscale structures - The SANS Toolbox.* National Institute of Standards and Technology. Center for Neutron Research., Gaithersburg, MD 20899-6102, 2010.

[17] A. Hasmy, E. Anglaret, M. Foret, J. Pelous, and R. Jullien. Small-angle neutron-scattering investigation of long-range correlations in silica aerogels: Simulations and experiments. *Phys. Rev. B: Condens. Matter. Phys.*, 50(9):6006–6016, 1994.

[18] A. Hasmy, M. Foret, J. Pelous, and R. Jullien. Small-angle neutron-scattering investigation of short-range correlations in fractal aerogels: Simulations and experiments. *Phys. Rev. B: Condens. Matter. Phys.*, 48(13):9345–9353, 1993.

[19] A. Hasmy and R. Jullien. Percolation in cluster-cluster aggregation processes. *Phys. Rev. E*, 53(2):1789–1794, 1996.

[20] A. Hasmy, R. Vacher, and R. Jullien. Small-angle scattering by fractal aggreagates: A numerical investigation of the crossover between the fractal regime and the porod regime. *Physical Review B.*, 50(2):1305–1308, 1994.

[21] Larry L. Hench and Jon K. West. The sol-gel process. *Chem. Rev.*, 90:33–72, 1990.

[22] Lawrence W. Hrubesh. Aerogel applications. *J.Non-Cryst. Solids*, 225:335–342, 1998.

[23] Arnaud E. Jacquin. Image coding based on a fractal theory of iterated contractive image transformations. *IEEE Transactions on Image Processing*, 1:18–30, 1992.

[24] R. Jullien and M. Kolb. Hierarchical model for chemically limited cluster-cluster aggregation. *J. Phys. A: Math Gen.*, 17:L639–L643, 1984.

[25] M. Kallala, R. Jullien, and B. Cabane. Crossover from gelation to precipitation. *Phys II France*, 2:7–25, 1992.

[26] Xin Li and Stephen E. Rankin. Multiscale dynamic monte carlo/continuum model of drying and nonideal polycondensation in sol-gel silica films. *AIChE J.*, 56(11):2946–2956, 2010.

[27] Ning Lu. *Fractal Imaging.* Academic Press, United States of America, 1997.

[28] A. Martucci, D. Buso, M.D. Monte, M. Guglielmi, C. Cantalini, and C. Sada. Nanostructured sol-gel silica thin films doped with nio and sno2 for gas sensing applications. *Journal of Materials Chemistry*, 14:2889–2895, 2004.

[29] R.M. Mazo. *Brownian Motion. Fluctuations, Dynamics and Applications.* Oxford University Press, New York, USA, 2002.

[30] R.L. Orbach. Dynamical properties of fractal networks: Scaling, numerical simulations, and physical realizations. *Rev. Mod. Phys.*, 66(2):381–443, 1994.

[31] Rakesh P. Patel, Nirav S. Purohit, and Ajay M. Suthar. An overview of silica aerogels. *International Journal of ChemTech Research*, 1(4):1052 – 1057, 2009.

[32] D. Pope. Nasa puts the heat on aerogels. *Ind. Physicist*, 3:13, 1997.

[33] J.S. Rivas-Murillo, M.E. Bachlechner, F.A. Campo, and E.J. Barbero. Structure and mechanical properties of silica aerogels and xerogels modeled by molecular dynamics simulation. *J. Non-Cryst. Solids*, 356:1325–1331, 2010.

[34] Clment Sanchez, Cdric Boissire, David Grosso, Christel Laberty, and Lionel Nicole. Design, synthesis, and properties of inorganic and hybrid thin films having periodically organized nanoporosity. *Chemistry of Materials*, 20(3):682–737, February 2008.

[35] Robert Sempéré, Daniel Bourret, Thierry Woignier, Jean Phalippou, and Rémi Jullien. Scaling approach to sintering of fractal matter. *Physical Review Letters*, 71(20):3307–3310, 1993.

[36] J. T. Seo, Q. Yang, S. Creekmore, B. Tabibi, D. Temple, S. Y. Kim, K. Yoo, A. Mott, M. Namkung, and S. S. Jung. Large pure refractive nonlinearity of nanostructure silica aerogel. *Applied Physics Letters*, 82:4444–4446, 2003.

[37] F. Spitzer. *Principles of Random Walk.* Springer-Verlag, New York, USA, 2nd edition, 2001.

[38] R. Vacher, T. Woignier, and J. Pelous. Structure and self-similarity of silica aerogels. *Phys. Rev. B: Condens. Matter. Phys.*, 37(11):6500–6503, 1988.

[39] E. Vinogradova, A. Moreno, H.V. Lara, and P. Bosch. Multi-fractal imaging and structural investigation of silica hydrogels and aerogels. *Silicon Chemistry*, 2:247–254, 2003.

[40] T. Woignier and F. Despetis. Mechanical properties of gel-derived materials. *J. Sol-Gel Sci. Technol.*, 19:163–169, 2000.

[41] T. Woignier, J. Reynes, A. Hafidi Alaoui, I. Beurroies, and J. Phalippou. Different kinds of structure in aerogels: relationships with the mechanical properties. *Journal of Non-crystalline Solids*, 241:45–52, 1998.

[42] V.V. Zosimov and L.M. Lyamshev. Fractals in wave processes. *Physics - Uspekhi*, 38(4):347–384, 1995.